Revisiting the Organic Template Model through the Microstructural Study of Shell Development in Pinctada margaritifera, the Polynesian Pearl Oyster

Jean-Pierre Cuif, Yannicke Dauphin, Gilles Luquet, Kadda Medjoubi, Andrea Somogyi, Alberto Pérez-Huerta

minerals

MDPI

Article

Revisiting the Organic Template Model through the Microstructural Study of Shell Development in *Pinctada margaritifera*, the Polynesian Pearl Oyster

Jean-Pierre Cuif [1,*], Yannicke Dauphin [2], Gilles Luquet [3], Kadda Medjoubi [4], Andrea Somogyi [4] and Alberto Perez-Huerta [5]

1 CR2P Centre de Recherche sur la Paléodiversité et les Paléoenvironnements, UMR 7207, Muséum National d'Histoire Naturelle CNRS MNHN Sorbonne-Université, 75005 Paris, France
2 ISYEB Institut de Systématique, Evolution, Biodiversité, UMR 7205 CNRS MNHN Sorbonne-Université EPHE Muséum National d'Histoire Naturelle, 75005 Paris, France; yannicke.dauphin@upmc.fr
3 BOREA Biologie des Organismes et Ecosystèmes Aquatiques, UMR 7208 CNRS MNHN Sorbonne-Université UA UCN IRD 207, Muséum National d'Histoire Naturelle, 75005 Paris, France; gilles.luquet@mnhn.fr
4 Nanoscopium beamline, Synchrotron Soleil, 91190 Saint Aubin, France; kadda.medjoubi@synchrotron-soleil.fr (K.M.); andrea.somogyi@synchrotron-soleil.fr (A.S.)
5 Department of Geological Sciences, The University of Alabama, Tuscaloosa, AL 35487, USA; aphuerta@ua.edu
* Correspondence: jean-pierre.cuif@orange.fr

Received: 21 June 2018; Accepted: 21 August 2018; Published: 25 August 2018

Abstract: A top-down approach to the mineralized structures and developmental steps that can be separated in the shells of *Pinctada margaritifera* was carried out. Detailed characterizations show that each of the two major layers usually taken into account (the outer prismatic layer and the inner nacreous layer) is actually the result of a complex process during which the microstructural patterns were progressively established. From its early growing stages in the deeper part of the periostracal grove up to the formation of the most inner nacreous layers, this species provides a demonstrative case study illustrating the leading role of specifically secreted organic structures as determinants of the crystallographic properties of the shell-building units. Gathering data established at various observational scales ranging from morphology to the nanometer level, this study allows for a reexamination of the recent and current biomineralization models.

Keywords: biomineralization; Mollusca; shell development; biocrystallization model

1. Introduction

Three decades only after the pioneering observations of shell microstructures by Bowerbank [1] and Carpenter [2,3], the paradoxical patterns of the calcareous hard parts built by many invertebrate groups were clearly apparent. Formation and structure of calcareous shells are not due to the calcification of the cells themselves; they should be interpreted as a secretion process [4]. This interpretation was not easily accepted, as illustrated by a famous one-decade long controversy with the opposing views of von Heider [5] and von Koch [6] about the origin of stony coral skeletons. Ten years later, Ogilvie [7] was still supporting a cellular calcification process (the von Heider's view), until the publication of Bourne's high-resolution observations [8] that definitely validated von Koch's conclusions. The progress in characterization methods (such as polarization microscopy and X-ray diffraction) has continuously increased the evidence of the paradoxical character of the skeletal units that build calcareous shells. Although crystallization always occurs outside the cells of the mineralizing organ (mantle of the mollusks, basal epithelium of the coral polyps, etc.), the calcareous units exhibit

species-specific well-defined morphologies, various three-dimensional arrangements, and individual crystalline behaviors with the additional particularity that the morphology of the crystalline units never corresponds to the idiomorphic pattern of the selected carbonate polymorph.

The first conceptual response to this intriguing blend of physical and biological properties relies on a parallel made between the arrangement of the crystalline units of the shells and the oriented development of crystals that may grow on the surface of some organic films, as exemplified by the Langmuir-Blodgett experiments. This process enables the production of single- or multilayer films with precise control of molecular orientations. As a result, thin organic polymers with specific structures and topologically controlled functional groups can be used as experimental frameworks, allowing the formation of layers of oriented crystalline particles when placed in appropriate chemical conditions. Mann [9] emphasized the possible transposition of this organic-inorganic process of crystallization to the living world, in which epithelial cell layers produce obviously controlled calcareous crystal-like units.

However, long before the occurrence of the template model, the presence of organic molecules associated with the mineral phase was recognized not only at the surface of the calcareous structures but within their whole thickness [10]. The following decades were marked by a series of biochemical analyses, mostly focusing on proteins, due to the rapid technical improvement of analytical devices. This analytical approach resulted in models emphasizing the possible relationships between molecular chains of acidic amino-acids acting as attractive substrates for Ca-carbonate ions [11,12]. In a reciprocal view, explaining the species-specific morphologies of Ca-carbonate crystals in living systems, the molecular attraction between Ca-carbonate lattices and organic compounds was hypothesized as a potential "crystal modeler" mechanism. In this concept, specifically secreted sets of organic compounds may act as growth modifiers through their fixation onto the normally growing crystal faces, inducing the modification of crystal shape and size. Thus, the concept of a continuous relationship between organic and mineral components was substituted to the template model to explain the formation and growth of calcareous biocrystals. This hypothesis was summarized as "shaping crystals with biomolecules" [13].

A new paradigm emerged when it was shown that, at the infra-micrometer level, the microstructural units made of aragonite or calcite do not exhibit the continuous mineral lattices that were suggested by both optical microscopy and usual scanning electron microscopy (Figure 1) [14,15].

Rare observations (e.g., [16,17]) had already shown that a granular structure of the mineral phase can be observed within some fossil samples. A series of secondary electron microscopy (SEM) views of growing surfaces and internal structures found in *Pinna* prisms (the reference model for biocrystals since Bowerbank [1] and Carpenter [2,3]) provided evidence of an unexpected fine structure and mode of growth, quite different from the structural patterns of a chemically produced crystal [18–21] (Figure 1c,d).

Figure 1e presents the first atomic forces microscopy (AFM) picture obtained from a calcareous prism of the outer shell layer of *Pinna nobilis* (Pelecypod Mollusca), fully confirming the SEM views. The dimensions of the granular units clearly establish the discontinuous organization of the mineral phase revealed in the 1980s by surface etching of the same type of material. Additionally, AFM phase contrast imaging (Figure 1f) shows the regular presence of a highly interactive layer around the grains, an interpretation supported by a previous series of pictures resulting from etching experiments in the 80s. Slight etching of the mineral phase produced a reticulate network of residual organic filaments ([14], Figure 1.6). First published for the description of the nacreous tablets of Cephalopods [20], this basically distinct and specific type of calcareous structure was extended to all biologically controlled Ca-carbonate [21]. These evidences contrast with the recently published model by De Yoreo and 13 associated physicists or chemists, in which particles forming the basic units of the crystallization process (including biominerals) exhibit a faceted morphology (mesocrystal style) at the end of their formation, whatever the diversity of their chemical trajectories ([22], Figure 1).

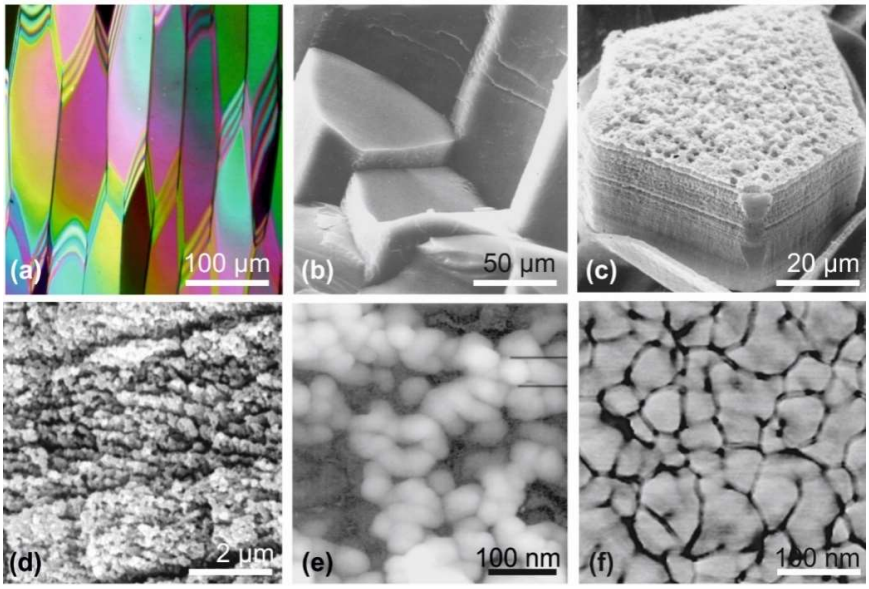

Figure 1. The earliest data on the reticulate structure of the calcareous biocrystals illustrated from *Pinna* shells (Pteriomorphid Bivalve). (**a**) Polarization microscopy (transmitted light) of a thin section in the prismatic structure (outer layer of the shell). Prisms are obliquely cut with respect to their growth axis. (**b**) Surface of a fractured prismatic layer. Note the perfectly compact aspect of the prismatic units consistent with polarized thin section. (**c**) Granular aspect of the growing surface of a prism whereas lateral faces show the layered mode of growth. (**d**) Evidence of the granular structure of the growth layers. (**e**) AFM view of the calcite prism ultrastructure. (**f**) Phase contrast imaging of the prism mineralized material. Credit pictures: (b,c) [15]; (d) [14].

Far from secondary, this difference is essential with respect to further steps in the process of the formation of crystalline units at the microstructural level. In chemically driven processes, a direct association of the basic particles through forces acting between their lateral faces allows for the development of mesocrystals, as schematized in the Cölfen-Antonietti model [23,24] (Figure A1).

Contrastingly, in the case of the granular units forming the microstructural components of the shells (and other calcareous biominerals), the absence of faceted surfaces implies a specific developmental process driving the production and assemblage of these spheroidal particles to produce the species-specific morphologies of the microstructural units. Major evidence for this biological control is given by the repeated observations (also exemplified below by the development of *Pinctada margaritifera* shell) that within a given species simultaneously producing two distinct shell layers built by morphologically different units, the basic grains are similar within each of these microstructural units. In other words, no morphological feature of the elementary grains can explain the morphological specificity of the skeletal units forming the shell layers.

Here, through a top-down approach of shell microstructure in *Pinctada margaritifera*, the Polynesian pearl oyster, an attempt is made to describe this controlled growth mode throughout the developmental sequence. Particular attention is paid to the presence and potential role of organic structures as it can be inferred from the time-based sequence of events that they control the three-dimensional growth of the shell.

2. Materials and Methods

Micro- and nanostructures were studied using thin sections, fractures, and polished etched surfaces under scanning electron microscopy (SEM) and atomic force microscopy (AFM). Electron microprobes (energy and wavelength dispersive spectrometry) were used for quantitative elemental chemical composition and distribution maps. Chemical distribution maps were also performed using

secondary ion mass spectrometer (NanoSIMS), time of flight (TOF-SIMS), and fluorescence X, while the chemical speciation was investigated by X-ray absorption near edge structure (microXANES). Details about the origin of the samples, preparative process, and setup of the diverse used techniques are given in the relevant publications listed in References [14,15,18–21,25–27]. Some sections were fixed, decalcified, and stained using Alcian blue solution; pieces of shells were first incubated for 15 min in a fixative solution containing 50% methanol and 7% acetic acid, then carefully washed in bi-distilled water before staining for 1 h in a solution containing 0.2% Alcian blue, 3% acetic acid, and 0.05 M $MgCl_2$ (pH 2.5). They were then incubated for 15 min in a destaining solution (3% acetic acid, 0.05 M $MgCl_2$), quickly washed, and air-dried before transmission light observations and X ray fluorescence (XRF) analysis.

The high analytical sensitivity XRF imaging was performed at the Nanoscopium beamline of SOLEIL Synchrotron (St. Aubin, France). The incident X-ray beam of 10 keV energy was focused by a Kirckpatrick-Baez mirror to a size of 0.3×0.3 μm^2 at the sample position. The elemental distribution maps were collected in continuous scanning (FLYSCAN) mode by two Si-drift detectors (Ketek) [28]. Information on the sample morphology was obtained by scanning transmission X-ray microscopy (STXM) by using a XPAD fast pixel-detector having 120×560 pixels with a pixel size of 130 μm.

3. Results

In contrast to the usual static description of the three distinct superimposed layers that make up *Pinctada* shells (periostracum, prismatic, and nacreous layers), a developmental investigation drew attention to the importance of the initial and transitional phases during which the characteristics of the microstructural units are established. This results in a different view of the shell, emphasizing the biological continuity between the activity of the mineralizing epithelium and the resulting microstructural growth steps. From the very beginning of shell formation in the deeper parts of the outer mantle grove up to the secretion of the nacreous tablets, these organic structures are key players in the determination of the structural patterns of shell components.

3.1. Origin and Growth Mode of the Flexible Shell That Predates the Prismatic Layer

The scaly aspect of the *Pinctada* shell is due to repeated retractions of the mantle within the shell, followed by a new onward growth phase. During these back-and-forth movements, the periostracum, this organic film that ensures continuity between the animal mantle and the shell, is fractured. One part remains attached to the animal and is withdrawn within the shell, whereas the other part remains attached to the outer surface of the shell. As a result, the outer side of the shell is marked by successive traces of the repeated shell closures (Figure 2b: arrows). A closer observation of these remains of the periostracum (Figure 2c,d) shows that they contain distant mineralized elements (Figure 2d), better visible at the growing edge of the shells, allowing the remains of the very last shell closure to be observed (Figure 2e–g). Without exception, these irregularly circular elements exhibit a distinct nodule in their center (Figure 2h–k).

The mode of growth of these structures is very specific. The mineral phase is deposited around the central nodule as concentric growth circles (Figure 3a–d), resulting in the formation of flat disks whose thickness does not exceed 3–4 μm (Figure 3e). The granular structure of the mineral phase is well visible in SEM view, on both natural and fractured surfaces (Figure 3d–f). The observation in transmitted polarized light clearly shows the crystallographic homogeneity of disks (Figure 2k). Attention must be drawn to the thickness of approximately 3 μm of these disks with respect to the polarization color. In spite of the high refractive index of calcite, the observed grey polarizing color (primary color) is in agreement with a thickness of 3 μm (see Figure 3e). More importantly, each disk behaves as a crystal-like unit in spite of its concentric growth mode, a pattern that has been previously established by a series of X-ray diffractions [25] (Figure A2). As the disks grow on the internal side of the periostracum, they are usually viewed perpendicularly to their surfaces, resulting in weak differences in grey colors, due to their slight differences in crystallographic orientations (Figure 3g).

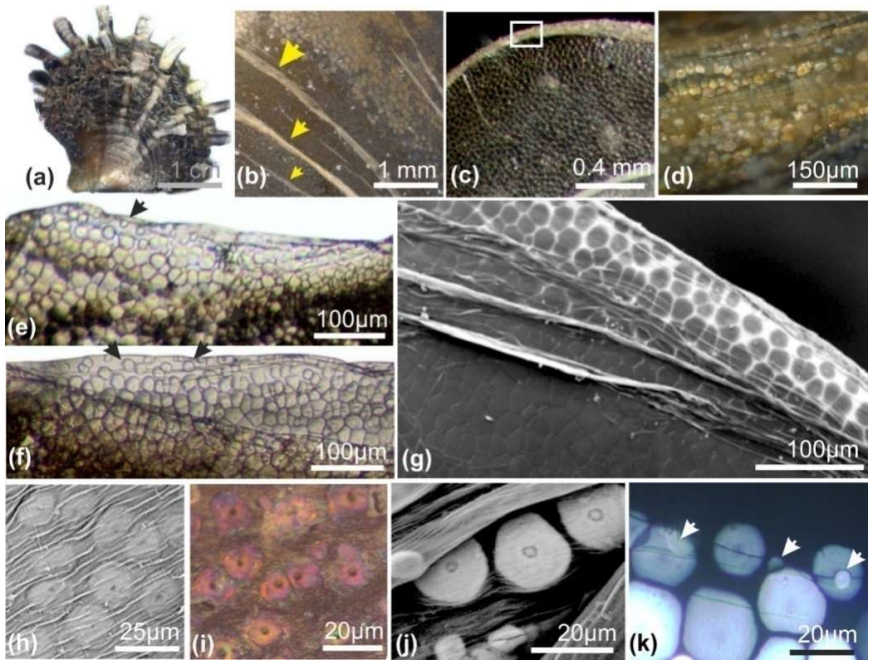

Figure 2. *Pinctada margaritifera:* discoid mineralized structures on the internal side of the periostracum. (**a**) Scaly aspect of the shell due to the series of back-and-forth movements of the mantle. (**b**,**c**) Remains of the periostracum on the outer surface of the shell. (**d**) Enlarged view of a periostracal remain: note the presence of the polarizing disks in the enrolled membrane. (**e**,**f**) Flat growing edge of the shell showing the round shaped disks at the forefront. (**g**) SEM view of an equivalent area. (**h**–**k**) Different equivalent views of the periostracal disks at the growing edge of the shell growth lamella. (**h**) Disks and central nodule viewed by SEM outer surface of the periostracum. (**i**) Optical microscopy (polarized episcopy). (**j**) SEM view of the folded periostracum showing the different growth statuses of the disks. (**k**) Equivalent area in transmitted polarized light. Note that the young disks (arrows) are apparently superposed to the older ones, due to periostracum folding. Credit pictures: (g,j) [25].

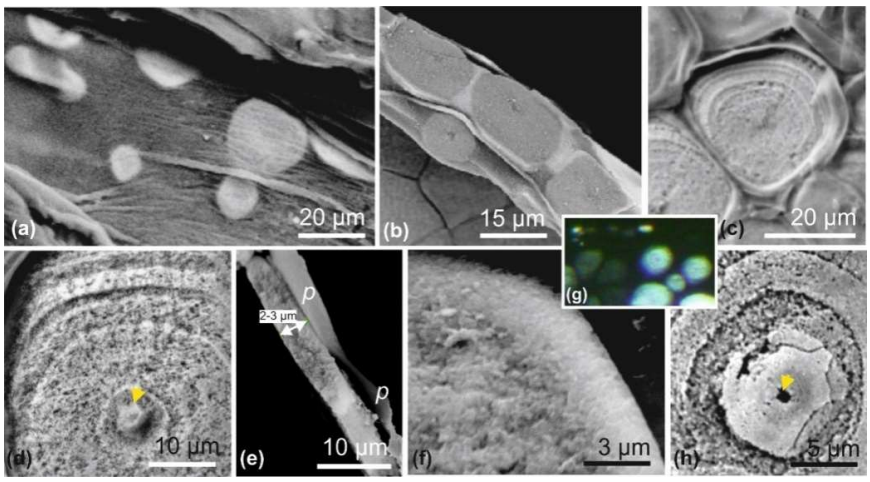

Figure 3. *Pinctada margaritifera*: disks development and structure. (**a**) Early mineralization stages of the disks. Note the parallel growth striation of the periostracum. (**b**) Almost final growth stages. (**c**,**d**) Evidence of concentric mineralization. Note the central nodule. (**e**) Growth of the disks is only bi-directional. Up to their last stages they remain thin structures about 3 µm thick. (**f**) Granular structure of the disks. (**g**) Differences in polarized transmitted light between neighbor disks (similar thickness) suggest distinct crystallographic orientations. (**h**) A partially decayed disk shows the empty place of the initial nodule. Credit pictures: (b,d) [25].

It should be noted that the central nodules are always visible in transmitted light but, when using SEM, the central nodules and concentric growth lines are visible only when looking at the external side of the periostracum. On the internal sides of the disks (opposite to the periostracum) central nodules and growth circles are generally not visible.

3.2. From Flexible to Rigid Shell: Integration of Periostracal Disks into a Polygonal Prismatic Network

At the end of the transit within the outer mantle grove, the periostracal flexible shell appears as a cluster of juxtaposed and rather irregular units (Figures 3h and 4a,b). Due to the continuous stepping growth of the periostracum, the mineralized units that have been produced in the deeper part of the grove and have grown during their transit arrive at the junction between the epithelial cells of the grove and the outer mantle surface ([25], (Figure 8 and Figure A3). There, they are subjected to an upside movement of the periostracum, leading the raw disk to become the new growing edge of the shell. At this turning point of shell formation, the mineralization is no longer ensured by the cells of the outer mantle grove but by the external cell layer of the mantle. This leads to two major consequences with respect to shell structure and formation: the development of polygonal envelopes of the prismatic units and the correlated setting of a new mode of growth.

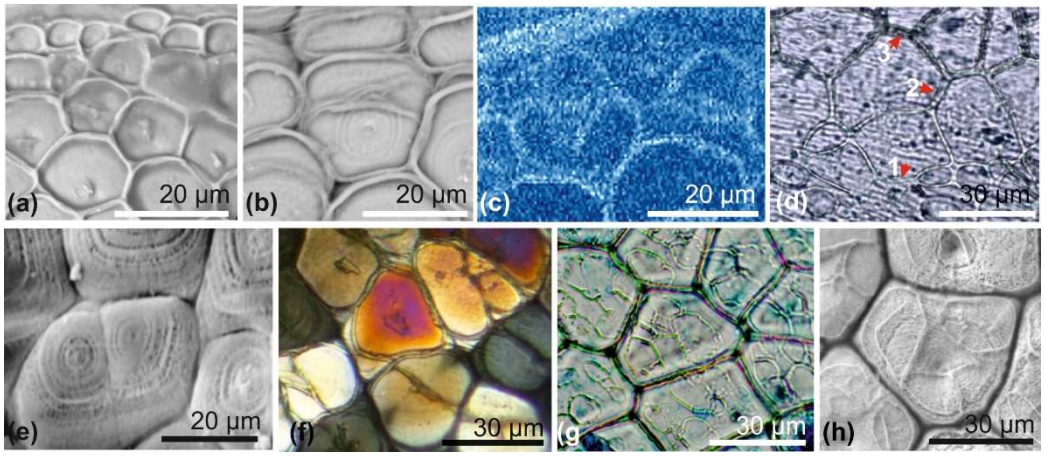

Figure 4. First step of the formation of the rigid shell of *Pinctada*. (**a**,**b**) SEM view of the periostracal units close to the end of their transit within the outer mantle grove; each is surrounded by an organic peripheral bulge formed by the mineralizing gel secreted by the mantle grove epithelium. (**c**) Synchrotron X-ray fluorescence shows evidence of Zn concentration in the individual bulge of the discs; see also Figure A4. (**d**) Beginning and progressive thickening (arrows 1 to 3) of the polygonal organic framework (Alcian Blue staining, decalcified preparation, transmitted light). Note in the background the parallel striation due to the pulsed periostracal growth. (**e**) Example of inclusion of two periostracal units (note their concentric individual development). (**f**) Transmitted polarized light. (**g**) Alcian Blue staining decalcified, transmitted light. Note the remains of the periostracal units inside polygons. (**h**) SEM view of an equivalent area. The calcified surface still bears the remains of the previous growth stage.

The diversity of sizes and irregularity of disk shapes contrast with the rather regular dimensions of the prisms in the adult shells. A regularization of the mean sizes and shapes occurs when the calcified units of the flexible periostracal shell are included in an organic polygonal network secreted by the external cell layer of the mantle. Figure 4 shows various images obtained by SEM, optical microscopy (transmitted natural and polarized lights), and synchrotron X-ray fluorescence, providing evidence that two or three of the neighbor periostracal disks may be included in a polygonal organic framework to form a new mineral unit with much more dimensional statistical regularity.

3.3. From Extensive Growth to Prism Thickness Increase: The Potential Role of the Marsh and Sass Membrane

The production of the polygonal organic framework not only regularizes the sizes and shapes of the shell building units but, most importantly, forms a key step in formation of the rigid shell.

Firstly, the remaining spaces between the periostracal disks are sealed by the deposition of calcareous material at the periphery of the disks (Figure 5a, arrows), clearly marking the passage from flexible to rigid shell. From this point the shell is no longer flexible, allowing the shell thickening step to begin.

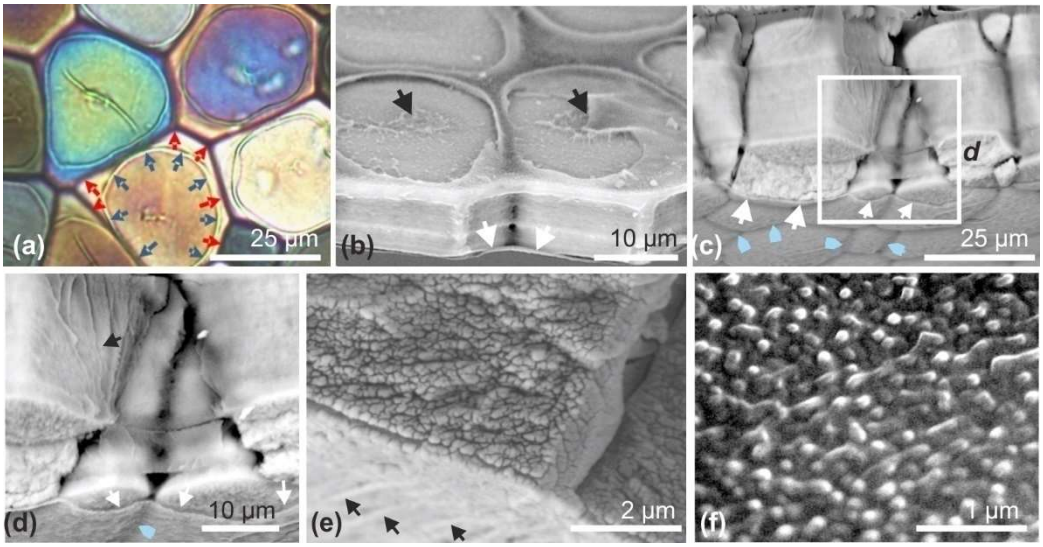

Figure 5. The newly formed prisms and the Marsh and Sass membrane on the internal side of the shell of *Pinctada*. (**a**) Sealing of the remaining spaces between disks. (**b**) Two neighbor prisms starting their inward growth by synchronic mineral deposition. On their outer surfaces, early decay of the periostracum reveals the positions of the initial nodules. Note the Marsh membrane on the internal side of the prisms. (**c**,**d**) Enlarged views of some prisms showing their internal side covered by the Marsh membrane. (**e**) Close adherence of the Marsh membrane to the mineralized material of the prism. Note the parallel striation of the outer side of the Marsh membrane (arrows). (**f**) Granular morphology of the Marsh membrane.

The microstructure of the calcareous units that grow onto the regularized surface of the shell edge reveals that the epithelial cell layer of the mantle follows a mineralization mode quite distinct from the previous calcification process by which the periostracal disks have been produced (Figure 5). Instead of an individual mode of growth typical for the periostracal disks, the mineral phase of these units is synchronically deposited within the newly produced polygonal framework (Figure 5b). Superposition of micrometer-thick growth layers ensures the inward growth of these units, increasing the thickness of the shell. As a result, these calcified units must be called prisms from this point owing to their growth mode, although at this stage their diameter largely exceeds their thickness.

A close observation of the basis of these newly formed prisms reveals the presence of a common membrane covering the whole internal surface of the growing structure (Figure 5b–e, arrows). This membrane is in close contact to the mineral phase of the prism. The limits of the growing prisms are visible on the external surface of the membrane (Figure 5c,d, blue arrows). A striking parallel can be made between these two figures and the observation of the "lamella" made by Bevelander and Nakahara [29] (Figure A6).

Two additional patterns are also visible: a parallel striation of the membrane (Figure 5e: arrows) and the granular organization of the membrane clearly visible from the SEM observations. This granular pattern was already emphasized by Marsh and Sass in their pioneering paper [30].

It is important to note that, owing to its position at the basis of the growing prisms, this membrane forms a permanent intermediate structure between the outer surface of the mineralizing epithelium of the mantle and the mineral phase of the prisms.

3.4. An Overall View of the Layered Growth of the Prisms from Micrometer to Nanometer Range

Figure 6a, obtained by polarization microscopy (transmitted light), provides us with colorful evidence of what occurs at the shell growing edge during the early stages of the prismatic layer formation. At the upper part of the view, the front line of the prismatic units exhibits slightly different grey colors, corresponding to a thickness of 3–4 µm of the calcite units, with distinct crystallographic orientations. The SEM view of the same area (Figure 6b,c) reveals their early developmental steps. The first occurrence of the Marsh membrane is visible on the inner side of the polygonal units, whereas on its outer side the regularly spaced lines illustrate the pulsed growth mode of the periostracum.

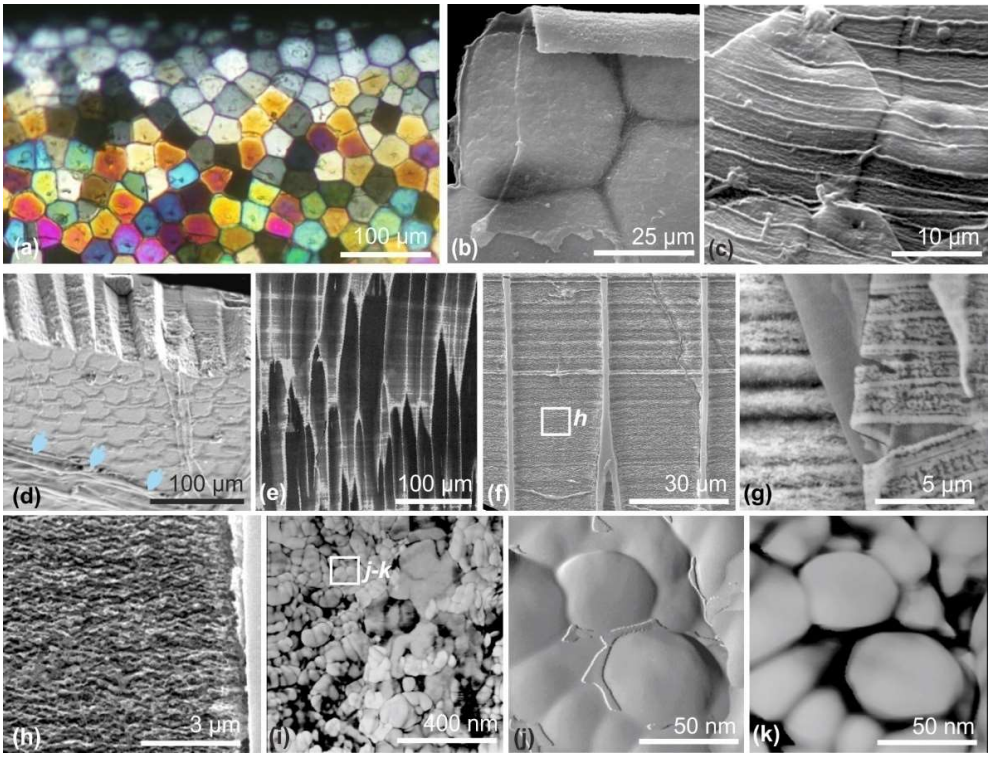

Figure 6. Layered growth of the prisms and morphology of the elementary mineralized units of *Pinctada*. (**a**) Transmitted polarized light on a large area of the shell growing edge. Thickness increase is assessed by the changing colors from the upper to lower part of the picture. Note the statistical dimensional regularity of the prism sections. (**b**,**c**) Inner (**b**) and outer (**c**) sides of the prisms at the shell growing edge. Note on the outer side the parallel stripes of the periostracum, indicating the pulsed secretion of the specialized cells in the deeper part of the outer grove of the mantle. (**d**) Internal surface of the shell prismatic layer; displaced Marsh membrane (blue arrows). (**e**) Slightly oblique surface in the prismatic layer showing the synchronic growth of the envelopes (laser confocal microscopy). (**f**) Layered growth mode of the mineralized phase. (**g**) Simultaneous growth of envelopes and mineral layers. (**h**) Discontinuous structure of the mineral material (SEM view). (**i**–**k**) AFM views of the mineralized material. (**j**) Amplitude image. (**k**) Phase contrast imaging. Credit pictures: (b,c,j,k) [21].

At the shell growing edge, the growth of the prisms is illustrated by the rapid color change of polarized light, passing from grey to the upper primary colors. Note the persistency of color diversity among prisms of the same ages (same distance from shell edge), suggesting that distinct crystallographic orientations visible among newly formed prisms are preserved during prism axial growth.

For prisms about 100 µm in length, the organic envelopes and the Marsh membrane (blue arrows) are clearly visible on the internal surface of the shell (Figure 6d). Note the slow morphological changes in prism morphology, also visible in Figure 6e. Enlarged views of the mineralized material confirm the layered mode of mineralization assessed by the perfect synchronism of mineral singularities between neighbor prisms (Figure 6f). As a rule, envelopes and mineralized material grow with the same layered mode as shown by the similar growth rhythm visible in the slightly decalcified fractured surface (Figure 6g). The discontinuity of the mineralized material is visible in the SEM pictures, but the true morphology of mineral particles can be clearly illustrated by AFM pictures only (Figure 6i–k).

Attention must be drawn to the complete absence of crystal faces on these basic components of the prisms. Phase contrast imaging (Figure 6k) emphasizes the distinct properties of the material located between the spheroidal units.

3.5. Time-Based Change of Prism Internal Structure

Prisms of *Pinctada margaritifera* exhibit two distinct and successive structural status (Figure 7). In their early stages, up to a length of about 120 to 150 µm, they grow as single-crystal-like units (calcite) by the superposition of about 2–3 µm thick growth layers that also comprise the formation of the polygonal organic network (prism envelopes) that grows accordingly. Figure 7b shows the successive growth layers after acidic etching. Longitudinal (Figure 7c) and transversal (Figure 7d) thin sections of these young prisms indicate a monocrystalline behavior.

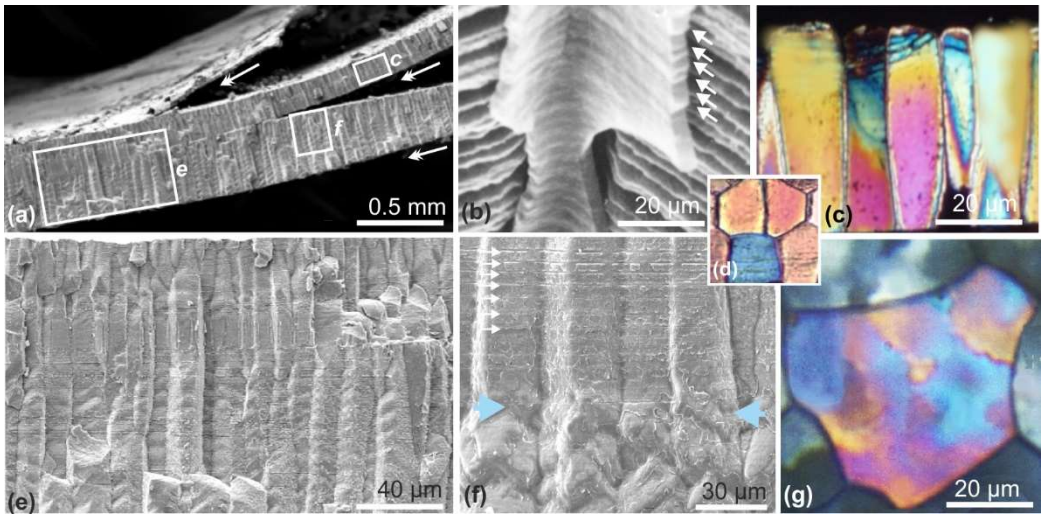

Figure 7. Shift from single-crystal-like units to polycrystalline organization of the calcite prisms in *Pinctada margaritifera*. (**a**) The shell stepping growth at the macro-scale; three scales of various thicknesses due to three mantle withdraws. (**b**) The stepping growth at the microscale seen by the synchronic growth of the envelopes and the mineral phase of the prisms. (**c**,**d**) Overall similarity in crystallographic orientation during early elongation of the prisms (about 200 µm). (**e**,**f**) The surface fracture of the shell reveals the morphological changes in prisms. (**g**) Diversity of crystal orientations in the second growth phase of the prisms.

Figure 7e shows the second stage, characterized by the presence of several crystalline units within a single envelope. This microstructural change is clearly visible by simple examination of prism morphologies on a fractured shell. Instead of flat prism surfaces in contact with each other by regular angles (Figure 7f, upper part), in this stage the surfaces of the prisms are marked by irregular nodules (Figure 7f, lower part). Thin sections made in such areas and observed in polarized light reveal that multiple crystalline orientations can be found within a given prism (Figure 7g), contrasting with the single-crystal appearance of the thin sections made in the upper part of the same prism (Figure 7d).

Also remarkable is the synchronism of the passage from single to polycrystalline status within a single shell scaly unit. Figure 7f shows the perfectly regular growth striation parallel to the shell surface visible on the upper part of four neighbor prisms and the simultaneity of the microstructural change leading to the production of polycrystalline units.

3.6. Sequence of Microstructural Events in the Formation of the Nacreous Layer

In contrast to a widely shared view, the spreading of the nacreous layer onto the prismatic internal surface is not the cause of the end of prism growth. Various converging data suggest that the end of prism growth is also a time-based process. An SEM view of the upper surface of the prisms shows a regression of the mineralizing area before the deposition of aragonite (Figure 8a,b). This correlates with biochemical changes in the prism mineralizing matrices (Figure 8c) [26]. Simultaneously, biochemical changes occur in the composition of the prism envelope, leading to the appearance of holes (Figure 8d).

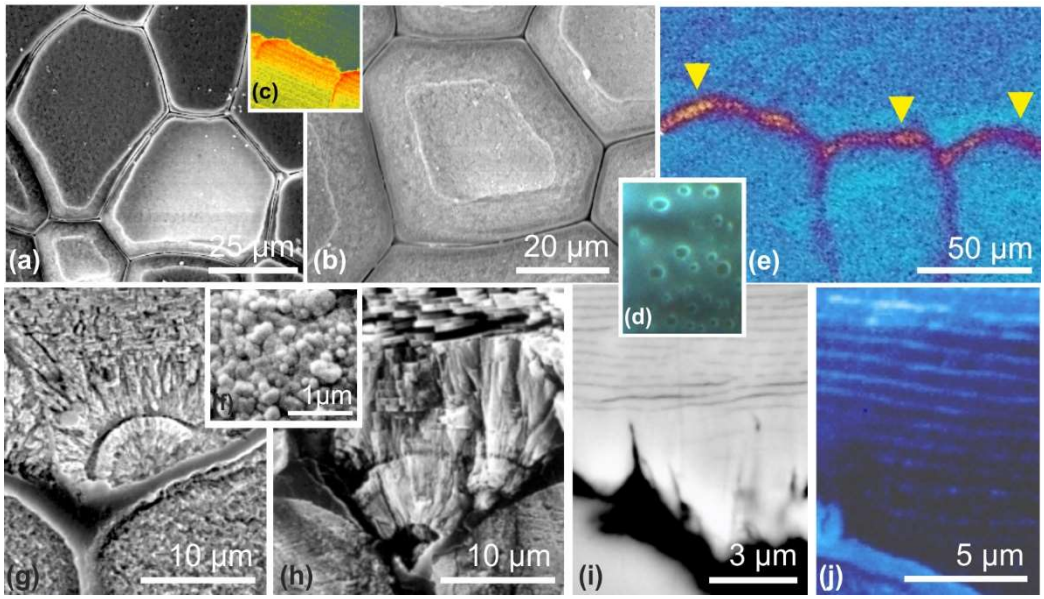

Figure 8. *Pinctada*: structural and biochemical changes during the major transitional phase in shell formation: occurrence of aragonite in a pre-nacreous phase. (**a**,**b**) Regression of the mineralizing membranes at the top of the prisms in the terminal growth phase. (**c**) Biochemical changes in the composition of the mineralizing layers (XANES mapping). (**d**) Holes in the prism envelopes (UV fluorescence). (**e**) Patchy aspect and specific composition of the organic (glycine) deposition onto the final surface of the prisms (TOF-SIMS mapping); note the difference from the prism envelopes. (**f**) Granular structure of early aragonite deposition on the organic membrane covering the prisms. (**g**,**h**) Spherulitic crystallization of aragonite on the initial aragonite deposition. (**i**,**j**) Progressive occurrence of nacreous membranes viewed in SEM backscattered mode and (**i**) NanoSIMS (**j**). Credit pictures: (c,j) [26], (e) [27].

The biochemical specificity of the organic deposition that covers the upper surface of the prismatic layer when the growth of this layer is finished has long been ignored. TOF-SIMS investigations have revealed its patchy deposition and locally variable composition (Figure 8e: arrows) [27].

In this transitional area, the occurrence of such a specific organic deposition is far from neutral as it provides a substrate for the primary deposition of aragonite. Noticeably, aragonite is not deposited immediately as nacre (i.e., mineral tablets surrounded by organic envelopes). Rather, the very early aragonite deposition consists of circular patches of very small granules (Figure 8f) followed by fibrous diverging fascicles or spherulites (Figure 8g,h).

The following step towards nacre formation is the occurrence of parallel organic membranes. Initially discontinuous, these parallel membranes (with a distance between them of about 1 µm or less) become rapidly continuous (Figure 8i). These membranes are essentially protein-made, as shown by NanoSIMS mapping (Figure 8j). Although it resembles a nacre organization, this microstructure still differs from true nacre as careful observation of the interval between the organic membranes reveals that the short mineral units between the membranes maintain the orientation of the underlying fibers (Figure 9a,b).

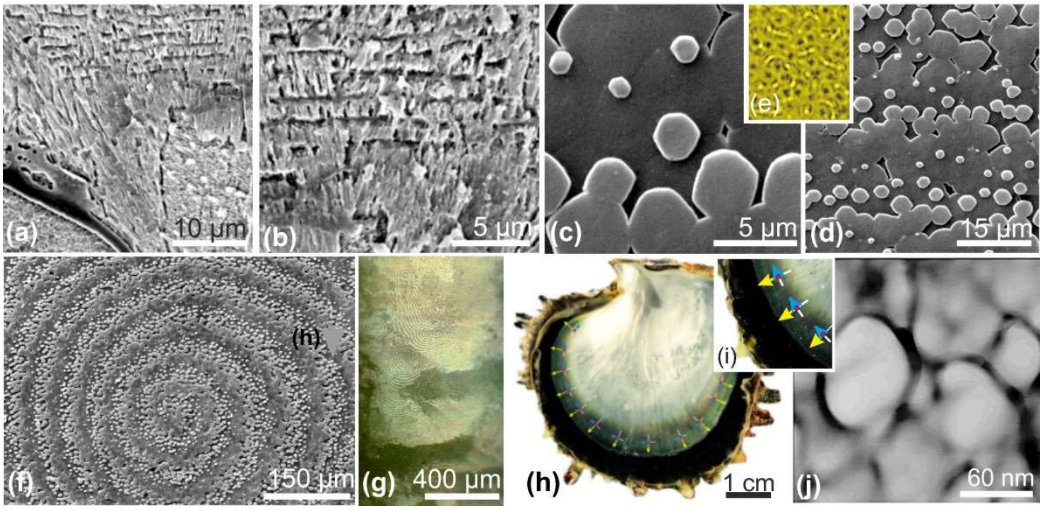

Figure 9. The two-phase process of nacre formation: from pre-nacre to nacreous tablets and overall crystallographic orientation of the nacreous layer of *Pinctada*. (**a**,**b**) Persistency of fibrous radial orientation between the parallel organic membranes. (**c**,**d**) Nacreous tablet growth and (**e**) Alcian blue staining of their initial nodules. (**f**) Regular spiral made by nacreous tablets and (**g**) most common irregular overall arrangement. (**h**,**i**) View of an inner surface of *Pinctada* shell showing crystallographic orientations of the nacreous tablets linked to the growth direction (yellow arrows: *a*, blue: *b*, red dots: *c* perpendicular to the shell surface). (**j**) Reticulate crystallization of the grains necessarily controlled at the overall shell level. Credit pictures: (c,d,f) [21].

True nacre is completely different in origin. It occurs when small organic nodules are deposited onto the organic membranes and act as centers of calcium carbonate deposition. The protein and sulfated proteoglycan composition of these nodules was shown by Nudelman et al. [31]. This implies the formation of a new specific generative area in the mantle epithelium producing flat crystals expending up to enter in mutual contact (Figure 9e,g). It must be noted that the growth of nacreous tablets is an oblique stepping process with respect to the direction of the nacreous layers. The initial nodules are linearly deposited on the distal area of the nacreous layer, creating a series of superposed layers that simultaneously spread onward and cover the fibrous aragonite areas. Finally, the complex aragonitic structure covers the internal surface of the calcite prismatic units.

Evidence of the overall control of this crystallization process has long been remarked [32]. *Pinctada margaritifera* produces rather circular shells. Using X-ray diffraction, Wada was able to show that the crystallographic orientation of nacreous tablets within a given shell is by no means a randomly distributed property. At the growing edge of the nacreous area, the crystallographic orientation of the nacreous tablets crystals is arranged in such way that the *c* axis is statistically perpendicular to the shell surface, the *a* and *b* axes being respectively parallel and perpendicular to the shell edge. In more internal areas, tablet groups in which the crystallographic orientations are rather similar are produced, whatever the global figure of the geometrical distribution may be.

4. Discussion: Ancient and Current Models in Light of Recent Microstructural Data

Starting with the initial deposition of organic nodules in the deeper part of the outer mantle grove and ending with the remarkably controlled arrangement of the nacreous tablets in the most internal areas, this overview of *Pinctada* shell development can be summarized in Figure 10. Attention is drawn to the series of metabolic events that lead to the formation of this shell, which is the typical representative of the "prismatic/nacreous" model, frequently used as a general model for calcification in Bivalves.

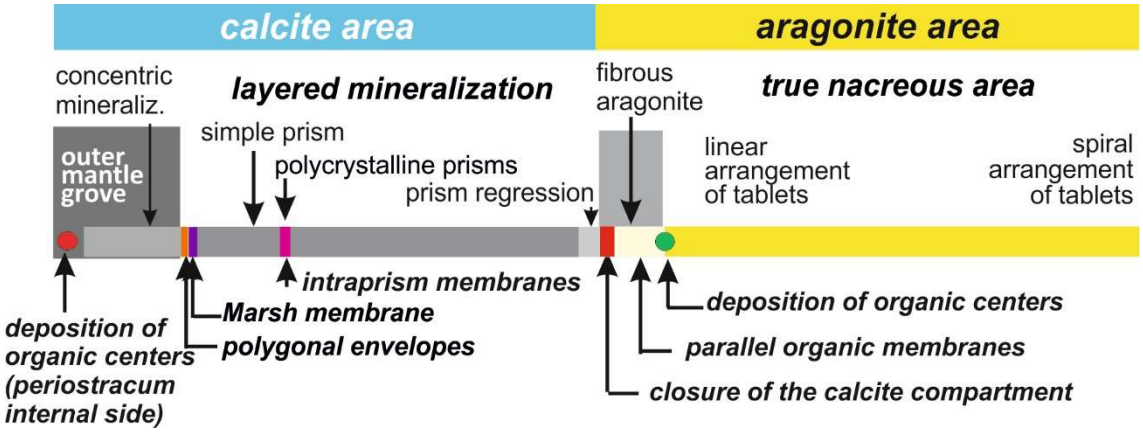

Figure 10. Sequence of the organic structures acting during *Pinctada* shell development.

Supported by the series of structural data from Section 3, this scheme allows for a reexamination of the literature current models (usually taking into account a limited part of the developmental sequence only), then a comparison of the origin and growth mode of the prismatic and nacreous layers, apparently very distinct under many respects, but showing also surprising similarities when considering the whole developmental history.

4.1. Recent Views about Shell Growing Edge

Although less thoroughly investigated than the nacreous layer, the growing edge of the shell has gained attention since the work of Wada ([32], Figure 8, p. 780), who presented a realistic approach of shell formation, observing a specific area predating the typical prismatic layer in *Pinctada fucata*. Wilbur ([33], p. 161), using Wada's data, then Taylor and Kennedy [34] considered these structures to be the result of a spherulitic crystallization process simultaneously producing the prismatic mineral structure and the organic envelopes through a single-phase mechanism. Admitting that prisms become polygonal by mutual contact, these authors considered that the growing mineral units produce the prism envelopes by "squeezing" the remaining organic components "as impurities to the edges of the growing crystals".

In a more recent investigation dealing with *Pinctada fucata* (the Japanese pearl oyster), Suzuki et al. [35] were able to characterize calcite in a thin section of disk still in place on the internal side of the periostracum using transmission electron microscopy and selected area electron diffraction (SAED).

The concentric crystallization described in the present paper modifies Wada's scheme. Undoubtedly, every growing unit appears as a crystal-like unit but it does not develop by spherulitic crystallization. Starting from an organic nodule and growing by the addition of concentric rings, the development of the periostracal disks appears as a remarkable example of organic/inorganic relationships, i.e., a first illustration of the organic template model in shell development. To date no data exists regarding molecular composition and the structure of the initial nodules that ensure the initial crystallization of the first calcite ring.

Crystallization of the disks by accretion of concentric rings contrasts with their single-crystal behavior. Note that if the disk crystallization followed the classical ionic-type process, these individually distant and freely growing disks would exhibit visible traces of the typical calcite regular faces. It must be emphasized that this never occurs, providing a demonstrative example of the biological effect exerted on the crystallization process, preventing the formation of faceted crystals at the supra-micrometric dimensional scale.

In the mesocrystal model of crystallization, the mutual attachment of faceted particles leads to faceted massive crystals (Figure A1). Distant from each other during their growth and consequently growing without mutual interaction, every disk should grow as a faceted crystal if the mesocrystal growth mode was followed during disk growth. Contrastingly, no trace of crystalline surface is visible in the disks, whatever the observational level, clearly establishing that attachment by lateral sides, as suggested in the De Yoreo et al. model [22], is not the mechanism at work in the formation of the disks.

Figure 4c shows that the periphery of every growing disk is marked by an important bulge whose particular chemical composition is illustrated in this paper by a single example: the concentration of zinc detected by synchrotron X-ray fluorescence mapping (Figures 4c and A4). Conclusively, the growth of periostracal disks provides an accessible case study of a species-specific biochemical matrix in which biologically controlled crystallization occurs. The importance of data regarding the composition of the organic medium in which the disks are growing cannot be overestimated.

Once started, the accretion of calcite rings increases the disk diameter and note must be made of the probable concomitance between the pulse growth of the disks and the stepping growth mode of periostracum acting as a conveyor-belt for these growing units. To date, no evidence has been found of a correlation between the pulse growth mode of the periostracum (assessed by parallel striation visible on the whole shell (see Figures 2h, 3c,d, 4d and 6c) and the stepping increases of disk diameters (Figure 3c,d). However, further observations on the growth mode of prisms and nacreous tablets in *Pinctada* shell contribute to such an interpretation.

4.2. Formation and Structural Evolution of the Prisms

Among the data gathered in Figure 4, Figure 4d offers a clear view of the second step in shell development. Viewed from the internal side of the periostracum (whose stepping growth striation is still visible in the background), this decalcified preparation clearly shows the occurrence of the polygonal organic framework that appears at the turning point of the periostracum (Figure A3). These polygons frequently gather two or three small irregular disks produced during the previous growth step. Figure 4h exemplifies the solid counterpart of Figure 4d; the calcareous surface still bears the peripheral remains of the periostracal calcification phase.

Both pictures point to the fact that the formation of prismatic envelopes is not simply due to the mutual contact of early calcifying units, as hypothesized by researchers long ago. Polygonal organic frameworks are specifically produced at the growing edge of the shell to increase its lateral dimensions. The transfer of crystallization from the disks to the prisms is assessed by the repeated observation of the mean-size regulation of microstructural units at the very beginning of the prismatic layer.

The formation of prisms by the inclusion of complex predating structures disproves the widely shared concept of a "self-assembly" model based on freely growing molecules moving in a fluid-filled extra-pallial space (exemplified in Figure A5). From Saleuddin and Petit [36] to Calvo-Iglesias [37], this concept avoids any microstructural investigation, the users being confident in the capability of the molecules to reach the right place at the appropriate time.

4.3. The Possible Function of the Marsh Membrane Following the Bevelander/Nakahara Model

The elongation of the prisms through repeated and synchronic adjunctions of envelopes and mineralized material is an additional evidence of the pulsed biomineralization mechanism at the global scale in *Pinctada* shell growth. Additionally, the rigorously synchronized deposition of these growth layers points to the key-role of the Marsh membrane in the crystallization process of the prisms.

It has long been noted that prisms maintain their individual crystallographic orientation during their axial growth. This is particularly obvious in *Pinna* prisms (the reference for the prismatic microstructures) as well as true for *Pinctada* prisms during their early developmental phase (Figure 7). This remarkable property contrasts with the repeated back-and-forth movement of the mantle epithelium that provides the chemical and biochemical components ensuring prism growth. As it is quite improbable that such crystallographic continuity of the prisms could rely on an exact repositioning of the mantle epithelium after each withdrawing phase, this could be the role of the Marsh membrane.

The point is that if the mantle epithelium withdraws at every shell closure, the Marsh membrane does not participate in this mantle retraction as it is closely adhered to the growing internal faces of the prisms. When the shell reopens and mineralizing activity restarts, it can be reasonably hypothesized that the Marsh membrane plays a key role as an intermediate active agent by ensuring the continuity of each prism crystallization.

This provides an additional evidence that the microstructure of the prisms cannot rely on the properties of their nanometer-sized structural units (the spheroidal grains) and some chemical attractive forces between their lateral faces that simply do not exist (Figure 6j,k). In contrast, the activity of the Marsh membrane in controlling the crystalline orientation of every prism suggests that the concept of an organic template should be adapted to the complexity of the molecular environments in which the layered crystallization of prisms occurs.

4.4. From Simple to Polycrystalline Prisms: A Counter Argument to the Concept of "Crystal-Growth Competition"

The key role of the Marsh membrane can be inferred from the structural changes that occur in the growth of *Pinctada* prisms: the passage from single-crystal to polycrystalline status. This seems to be a rare phenomenon, possibly specific to *Pinctada* (see also [38]). The patterns illustrated in Figure 7 clearly show the intriguing crystallographic changes that synchronically occur in the prisms after a given period of growth as a single crystal.

Crystal-growth competition is a widely shared concept based on the argument that the growth of a given crystal is easier if its major growth axis (e.g., the *c* axis for calcite) is oriented in conformity with the geometrical organization of the shell (i.e., perpendicular to the shell surface). This concept obviously leads to a reduction of the number of prisms.

What occurs in the prismatic layer of a *Pinctada margaritifera* does not support such an interpretation. After a "single-crystal" period of growth, the prisms become polycrystalline. It is difficult to understand this phenomenon in the concept of a moving mineralizing epithelium that simultaneously produces prisms with a single-crystal structure and others with different organization. A time-based modification of the biochemical activity of the Marsh membrane resulting in the production of polycrystal prisms (instead of single) could be the origin of this distinct crystallization pattern. Actually, what occurs at the end of the prismatic area clearly supports the interpretation that aging of the Marsh membrane modifies its activity and has a detectable influence on prism growth.

It is a commonly shared view that the growth of the calcite prisms is interrupted by the onward spreading of the nacreous layer. Actually, converging data have shown that the end of prism biomineralization predates coverage of the prism layer surface [25]. Reduction of the Marsh membrane activity is assessed by the reduction of the prism mineralizing surfaces (Figure 8a,b) with detectable modification of the composition of the mineralizing matrices (Figure 8c) of envelope composition (Figure 8d). Formation of nacre does not prevent prism growth because end of the biochemical and crystallization activity of the prismatic area opens the way to the major microstructural change that subsequently occurs in shell formation.

4.5. From Prisms to Nacre: The Increasing Control Exerted on Aragonite Mineralization

It has long been noted that calcite and aragonite compartments of *Pinctada* shells are carefully separated by an organic membrane. Until the biochemical characterization of this membrane by

TOF-SIMS mapping (Figure 8e), it was considered as a simple expansion of the prism envelopes, carefully closing the calcite compartment before nacre deposition.

Figure 8e leads to a completely different interpretation. Instead of a simple separative role, the biochemical composition of this membrane suggests that it could be an active factor in occurrence of the first aragonite deposition. Figure 8f–h provides evidence of aragonite localized precipitation onto this membrane, whose irregular composition corresponds to the patchy deposition of aragonite. Figure 8f shows the granular structure of the very initial aragonite. There is no indication of a more precise biological control at this stage. Further steps consist in the repeated production of layered aragonite that takes a fibrous habitus, close to what can be seen in sedimentary precipitations.

With respect to biomineralization models, there is little doubt that the prism covering membrane acts as a mineralization substrate, though no organizational factor is present at that time to drive the aragonite grains up to the formation of morphologically specific units. Even the occurrence of parallel membranes (mostly protein, Figure 8i,j) does not influence aragonite deposition; Figure 9a,b reveals that between the parallel membranes the direction of the diverging fibers is preserved.

The phase of fibrous aragonite mineralization ends with the occurrence of small organic nodules, whose composition is now established [27]. With respect to mineralization models, the deposition of these nodules strikingly resembles the occurrence of the central nodules in the outer mantle grove (S3: *oc*), around which the calcite disks grow. From this viewpoint, the deposition of the central nodules of nacreous tablets can be interpreted as a second occurrence of crystallization centers, the role of which is potentially comparable in both prisms and nacre. However, the impressive results obtained by Wada [32], summarized here in Figures 9f–i and A7, demonstrate that the control of the crystallographic orientation of the nacre tablets is much more extensive than that of prism crystallization. Whatever the complexity of the overall figures formed by the spatial arrangement of the nacreous tablets, Wada was able to show that their *c* axis is perpendicular to the surface of the nacreous layer, whereas the *a* and *b* axes are oriented with respect to the overall growth directions of the shell(Figure 9i). The value of this result is shown by Wada's investigations carried out on different nacre-producing species. No exception was found to this pattern, demonstrating a highly significant example of biological control exerted over crystallization.

In spite of this difference, attention must be drawn to the gathered evidences that prisms and nacre, frequently pictured as directly produced shell building units (in a static description of shell microstructures), do not crystallize from freely moving molecules finding their way within a huge fluid-filled volume. Realistic reconstructions of shells must take into account the long and specifically organized preparative phases that predate the occurrence of the typical calcite and aragonite crystal-like units.

5. Conclusions

1. Microstructural investigation applied to the shell of *Pinctada margaritifera* reveals a sequence of growth steps in which organic structures play a key role by driving the formation and spatial arrangements of the mineralized units. With specific conditions for calcite prisms and nacreous tablets, structural observations suggest that the template interaction between organic structures and deposited minerals represents the organizational factor responsible for shell microstructures.
2. Up to the highest resolution levels, no trace of crystalline surface is visible in the shell building units, rendering irrelevant any model in which the formation of the microstructural units occurs by the side accretion of faceted pre-existing microcrystals.
3. In contrast to the "self-assembly" models, which consider that prisms and nacre are built through the movement of free molecules within a fluid-filled chamber, specific preparative structures can be identified, creating appropriate substrates for the development of prisms and nacre biomineralization.

Author Contributions: J.P.C. conceived, wrote the original draft and finalized the manuscript. All authors contributed to the writing and editing of the paper. A.S. and K.M. designed the synchrotron XFR experiments and

interpreted the results. J.P.C., Y.D. and G.L. selected and prepared the samples. J.P.C. performed SEM observations. Y.D. performed AFM observations.

Funding: This research was supported by a SYNTHESYS grant, the financial support of the French ANR through contract ANR-06-BLAN-0233 (biocrystal), ESRF grants (EC24, EC208), EU-IHP programme SYNTHESYS, GB-TAF NHM, and by the ESF-EuroCores-EuroMinScI-BioCalc project, and a SOLEIL grant (20170784).

Acknowledgments: The authors are grateful to several Polynesian people who contribute to this investigation by providing us with *Pinctada* specimens collected alive, then immediately preserved and sent to us in relevant conditions. Dominique DEVAUX, pearl producer at Rikitea (Gambier archipelago), Gabriel HAUMANI, DRMM biological station at Takapoto (Tuamotu archipelago), and Cedrik LO, Research and innovation in perliculture at the Direction des Ressources Marines et Minières de Polynésie and Mereani BELLAIS (DRMM station at Vairao) have made this research possible.

Conflicts of Interest: The authors declare no conflict of interest. The funders had no role in the design of the study; in the interpretation of data; in the writing of the manuscript, and in the decision to publish the results.

Appendix A

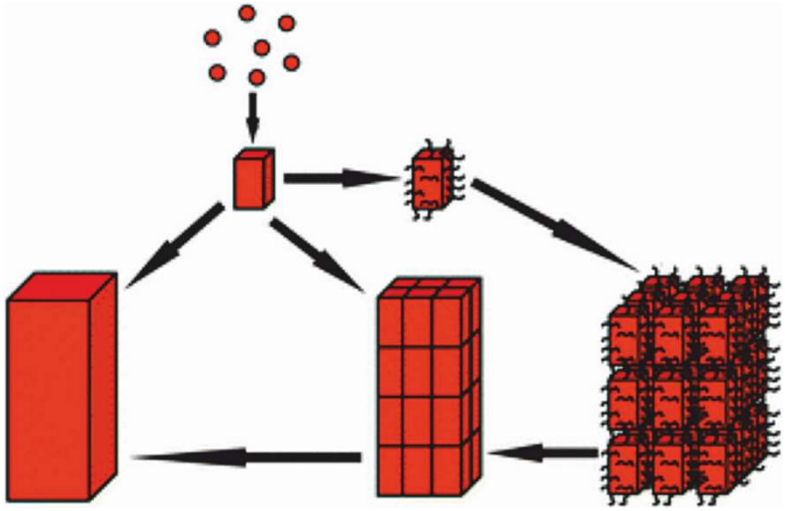

Figure A1. Scheme of mesocrystal formation by accretion of small crystalline units. Attraction due to chemical forces between their crystalline faces results in formation of the massive crystal. Credit picture [23].

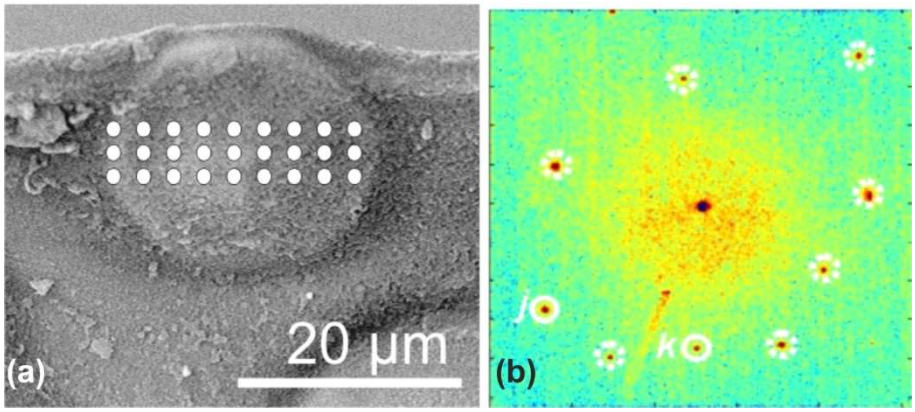

Figure A2. Disk at the growing edge of a *Pinctada margaritifera* shell showing the 3 × 9 X-ray diffraction spots **(a)** resulting in a single-crystal like diagram (**b**). Origin ESRF Grenoble, ID 13, operator: M. Burghammer. Credit picture [25].

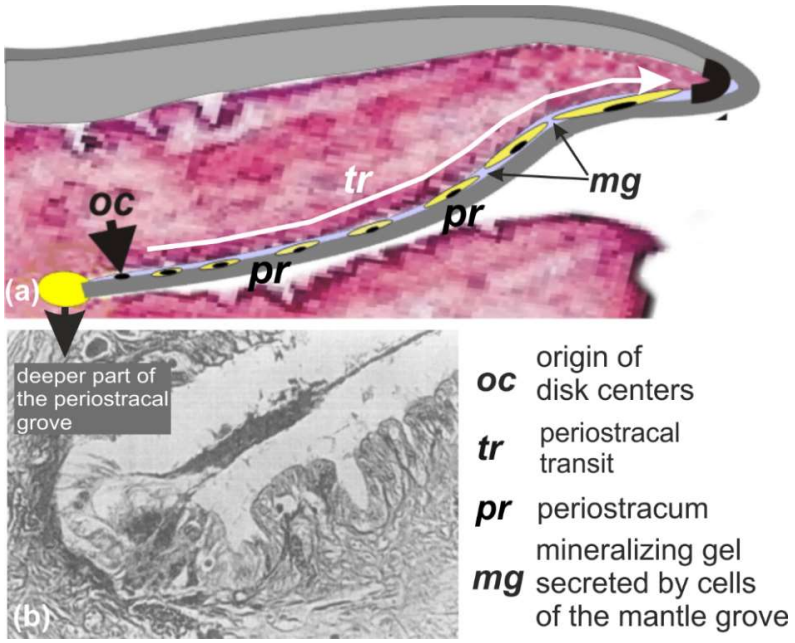

Figure A3. Scheme of the outer mantle grove (**a**) at growing edge of a*Pinctada margaritifera* shell cut perpendicular to shell surface. All along the animal life, periostracum is produced by a group of specialized cells (**b**). Through a pulsed secretion mode assessed by parallel striation (Figure 6c), the resulting membrane acts as a conveyor-belt for disks that grow by accretion of calcite rings around initial organic nodules deposited onto the internal side of the periostracal membrane. The black curved line shows the point where the disks are incorporated into the shell, becoming the fore-front of the solid shell. Credit pictures (a) Cuif and Dauphin, redrawn from Proceedings of the 14th Biomineralization meeting, Tsukuba, Japan, in press; b: [39].

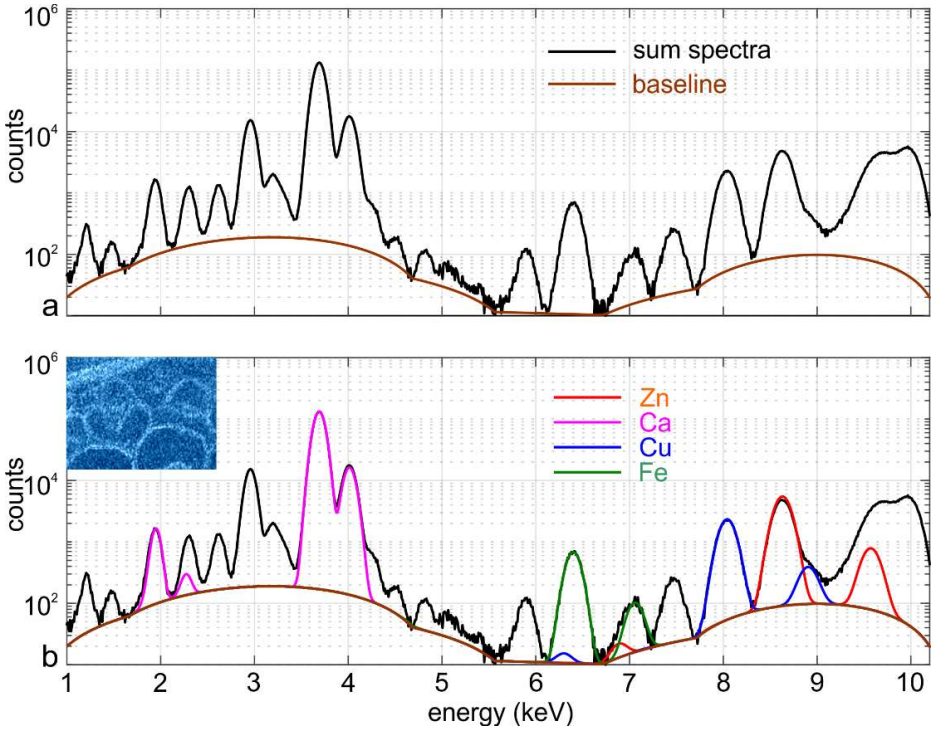

Figure A4. (**a**) Total XRF spectrum from Figure 4c. (**b**) Elemental peaks deconvolution showing the presence of Cu and Zn in the growing edge of *Pinctada*.

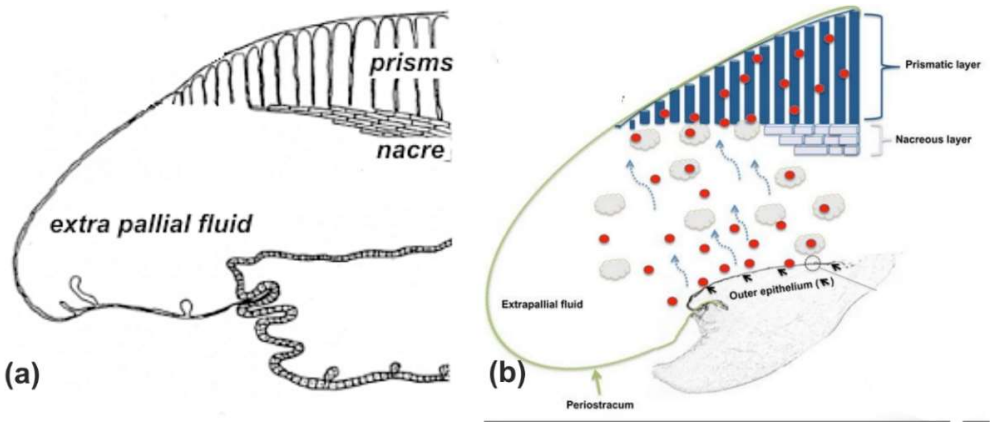

Figure A5. Models of fluid-filled extra-pallial chambers in which moving molecules go to the right places to build the shell layers. (**a**) Model from Saleuddin and Petit [36]. (**b**) Model from Saleuddin and Wilbur [37]. Credit pictures (a): [36]; (b): [37].

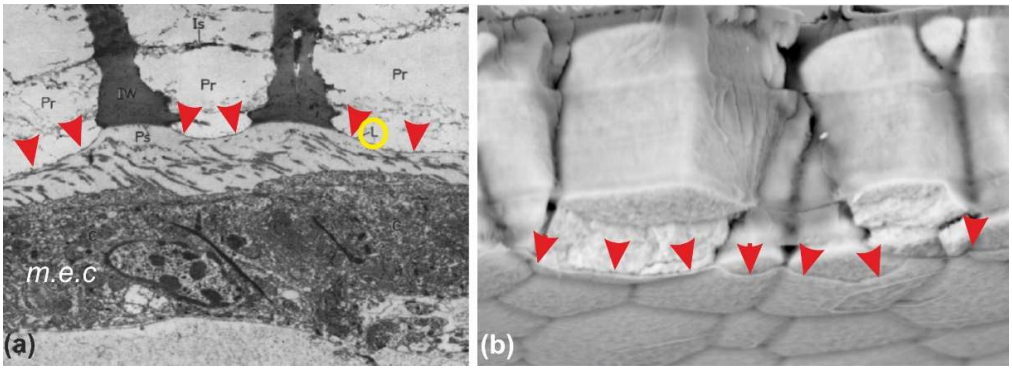

Figure A6. Comparison of the Bevelander and Nakahara figure (**a**) Transmission electron microscopy with a SEM view of a fractured shell of *Pinctada margaritifera*, showing prisms and inner surface of the prismatic layer. Secretions of the mantle epithelial cell layer (*m.e.c*) are separated from the mineralized prisms by the "lamella" (L in [29]), i.e., exactly the place of the Mash and Sass membrane. (**b**) Equivalent membrane is clearly visible at the basis of the prismatic layer in *P. margaritifera.* Credit pictures (a): [29]; (b): Cuif and Dauphin, Proceedings of the 14th Biomineralization meeting, Tsukuba Japan, in press.

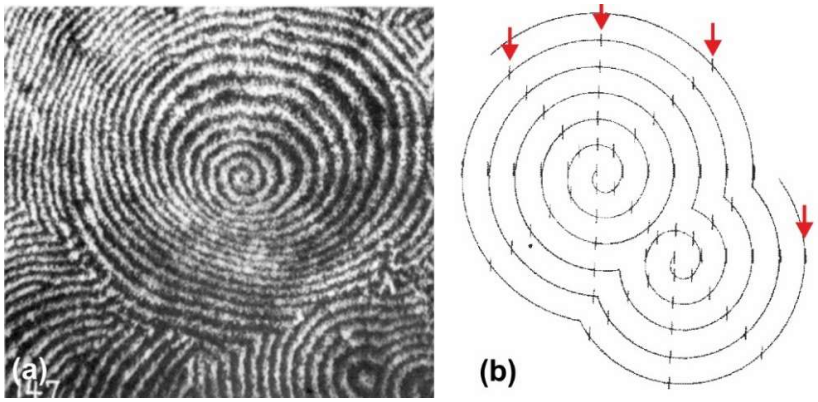

Figure A7. The Wada's figure showing large scale figures made by arrangement of nacreous tablets (**a**) in which parallel crystal orientations is globally maintained (**b**). Note that looking at the whole-shell level orientation of nacreous tablets follows the morphology of the shell growing edge. Credit pictures: [32].

References

1. Bowerbank, J.S. On the structure of the shells of molluscan and conchyferous animals. *Trans. Microsc. Soc. Lond.* **1844**, *1*, 123–152. [CrossRef]
2. Carpenter, W. On the microscopic structure of shells. Part I. *Br. Assoc. Adv. Sci.* **1844**, *14*, 1–24.
3. Carpenter, W. On the microscopic structure of shells. Part II. *Br. Assoc. Adv. Sci.* **1847**, *17*, 93–134.
4. Huxley, T.H. On the classification and the distribution of the crayfishes. *Proc. Zool. Soc. Lond.* **1879**, *46*, 751–788. [CrossRef]
5. Von Heider, A.R. Korallenstudien. *Zeitsch. Wissensch. Zoolog.* **1886**, *46*, 507–535.
6. Von Koch, G. Ueber das Verhältniss von Skelet und Weichtheilenbei den Madreporaren. *Morph. Jahrb.* **1886**, *12*, 154–162.
7. Ogilvie, M.M. Microscopic and systematic study of Madreporarian types of corals. *Phil. Trans. R. Soc. Lond.* **1896**, *B187*, 83–345. [CrossRef]
8. Bourne, G.C. Studies on the structure and formation of the calcareous skeleton of the Anthozoa. *Quart. J. Microsc. Sci.* **1899**, *41*, 499–547.
9. Mann, S. *Biomineralization: Principles and Concept in Bioinorganic Materials Chemistry*; Oxford UniversityPress: Oxford, UK, 2001; p. 210.
10. Grégoire, C.; Duchateau, G.; Florkin, M. La trame protidique des nacres et des perles. *Ann. Inst. Océanogr.* **1955**, *31*, 1–36.
11. Weiner, S. Aspartic acid-rich proteins: Major components of the soluble organic matrix of mollusk shells. *Calcif. Tissue Int.* **1979**, *29*, 163–167. [CrossRef] [PubMed]
12. Weiner, S.; Addadi, L. Acidic macromolecules of mineralized tissues: The controllers of crystal formation. *Trends Biochem. Sci.* **1991**, *16*, 252–256. [CrossRef]
13. De Yoreo, J.J.; Dove, P.M. Shaping crystals with biomolecules. *Science* **2004**, *306*, 1031–1302. [CrossRef] [PubMed]
14. Cuif, J.P.; Dauphin, Y.; Denis, A.; Gaspard, D.; Keller, J.P. Continuité et périodicité du réseau organique intra-prismatique dans le test de *Pinna muricata* L. (Lamellibranche). *CR Acad. Sci. Paris* **1980**, *290*, 759–762.
15. Cuif, J.P.; Denis, A.; Gaspard, D. Recherche d'une méthode d'analyse ultrastructurale des tests carbonatés d'Invertébrés. *Bull. Soc. Géol. Fr.* **1981**, *7*, 525–534. [CrossRef]
16. Mutvei, H. The nacreous layer in *Mytilus*, *Nucula*, and *Unio* (Bivalvia). *Calcif. Tissue Res.* **1977**, *24*, 11–18. [CrossRef] [PubMed]
17. Mutvei, H. Ultrastructure of the mineral and organic components of molluscan nacreous layers. *Biomineralization* **1970**, *2*, 48–72.
18. Cuif, J.P.; Dauphin, Y.; Denis, A.; Gaspard, D.; Keller, J.P. Étude des caractéristiques de la phase minérale dans les structures prismatiques du test de quelques Mollusques. *Bull. Mus. Natl. Hist. Nat. Paris* **1983**, *5*, 679–717.
19. Cuif, J.P.; Dauphin, Y.; Nehrke, G.; Nouet, J.; Perez-Huerta, A. Layered growth and crystallization in calcareous biominerals: Impact of structural and chemical evidence on two major concepts in invertebrate biomineralization studies. *Minerals* **2012**, *2*, 11–39. [CrossRef]
20. Dauphin, Y. Nanostructures de la nacre des tests de céphalopodes actuels. *Paläont. Zeit.* **2001**, *75*, 113–122. [CrossRef]
21. Cuif, J.P.; Dauphin, Y.; Sorauf, J.E. *Biominerals and Fossils through Time*; Cambridge University Press: Cambridge, UK, 2011; p. 490.
22. De Yoreo, J.J.; Gilbert, P.; Sommerdjik, N.; Penn, R.L.; Whitelam, S.; Joester, D.; Zhang, H.; Rimer, J.D.; Navrotsky, A.; Banfield, J.F.; et al. Crystallization by particle attachment in synthetic, biogenic, and geologic environments. *Science* **2015**, *349*. [CrossRef] [PubMed]
23. Cölfen, H.; Antonietti, M. *Mesocrystals and Nonclassical Crystallization*; John Wiley and Sons: Chichester, UK, 2008; ISBN 078-0-470-02981-7.
24. Niederberger, M.; Cölfen, H. Oriented attachment and mesocrystals: Non-classical crystallization mechanisms based on nanoparticle assembly. *Phys. Chem. Chem. Phys.* **2006**, *8*, 3271–3287. [CrossRef] [PubMed]

25. Cuif, J.P.; Burghammer, M.; Chamard, V.; Dauphin, Y.; Godard, P.; Le Moullac, G.; Nehrke, G.; Perez-Huerta, A. Evidence of a biological control over origin, growth and end of the calcite prisms in the shells of *Pinctada margaritifera* (Pelecypod, Pterioidea). *Minerals* **2014**, *4*, 815–834. [CrossRef]
26. Dauphin, Y.; Ball, A.D.; Cotte, M.; Cuif, J.P.; Meibom, A.; Salomé, M.; Susini, J.; Williams, C.T. Structure and composition of the nacre-prism transition in the shell of *Pinctada margaritifera* (Mollusca, Bivalvia). *Anal. Bioanal. Chem.* **2008**, *390*, 1659–1669. [CrossRef] [PubMed]
27. Farre, B.; Brunelle, A.; Laprévote, O.; Cuif, J.P.; Williams, C.T.; Dauphin, Y. Shell layers of the black-lip pearl oyster *Pinctada margaritifera*: Matching microstructure and composition. *Comp. Biochem. Physiol.* **2011**, *159*, 131–139. [CrossRef] [PubMed]
28. Somogyi, A.; Medjoubi, K.; Baranton, G.; Le Roux, V.; Ribbens, M.; Polack, F.; Philippot, P.; Samama, J.P. Optical design and multi-length-scale scanning spectro-microscopy possibilities at the Nanoscopium beamline of Synchrotron Soleil. *J. Synchrotron Rad.* **2015**, *22*, 1118–1129. [CrossRef] [PubMed]
29. Bevelander, G.; Nakahara, H. Compartment and envelope formation in the process of biological mineralization. In *The Mechanisms of Biomineralization in Animals and Plants*; Omori, M., Watabe, N., Eds.; Tokai University Press: Kanagawa, Japan, 1980; pp. 19–27.
30. Marsh, M.E.; Sass, R.L. Phosphoprotein particles: Calcium and inorganic phosphate binding structures. *Biochemistry* **1984**, *23*, 1448–1456. [CrossRef] [PubMed]
31. Nudelman, F.; Gotliv, B.A.; Addadi, L.; Weiner, S. Mollusk shell formation: Mapping the distribution of organic matrix components underlying a single aragonitic tablet in nacre. *J. Struct. Biol.* **2006**, *153*, 176–187. [CrossRef] [PubMed]
32. Wada, K. Crystal growth of molluscan shells. *Bull. Natl. Pearl Res. Lab.* **1961**, *36*, 703–828.
33. Wilbur, K.M. Shell formation and regeneration. In *Physiology of Mollusca*; Wilbur, K.M., Owen, G., Eds.; Academic Press: New York, NY, USA; London, UK, 1964; Volume 1, pp. 243–282.
34. Taylor, J.D.; Kennedy, W.J. The influence of the periostracum on the shell structure of bivalve Molluscs. *Calcif. Tissue Res.* **1969**, *3*, 274–283. [CrossRef] [PubMed]
35. Suzuki, M.; Nakayama, S.; Nagasawa, H.; Kogure, T. Initial formation of calcite crystals in the thin prismatic layer with the periostracum of *Pinctada fucata*. *Micron* **2013**, *45*, 136–139. [CrossRef] [PubMed]
36. Saleuddin, A.S.M.; Petit, H. The mode of formation and the structure of the periostracum. In *The Mollusca*; Saleuddin, A.S.M., Wilbur, K.M., Eds.; Academic Press: New York, NY, USA, 1983; pp. 199–234.
37. Iglesias, J.; Pérez-Estévez, D.; Lorenzo-Abalde, S.; Sánchez-Correa, B.; Quiroga María, I.; Fuentes José, M.; González-Fernández, A. Characterization of a monoclonal antibody directed against *Mytilus spp.* larvae reveals an antigen involved in shell biomineralization. *PLoS ONE* **2016**, *11*, e0152210. [CrossRef]
38. Okumura, T.; Suzuki, M.; Nagasawa, H.; Kogure, T. Characteristics of biogenic calcite in the prismatic layer of a pearl oyster, *Pinctada fucata*. *Micron* **2010**, *41*, 821–826. [CrossRef] [PubMed]
39. Jabbour-Zahab, J.; Chagot, D.; Blanc, F.; Grizel, H. Mantle histology, histochemistry and ultrastructure of the pearl oyster *Pinctada margaritifera* (L.). *Aquat. Living Res.* **1992**, *5*, 287–298. [CrossRef]